RSC Advances

ROYAL SOCIETY OF CHEMISTRY

www.rsc.org/advances

Cite this: DOI: 10.1039/c0xx00000x

www.rsc.org/xxxxxx

ARTICLE TYPE

Branched Peptide with Three Histidines for the Promotion of Cu^{II} Binding in a Wide pH Range – Complementary Potentiometric, Spectroscopic and Electrochemical Studies

Łukasz Szyrwiel[a,b]*, József S. Pap[c]*, Łukasz Szczukowski[b], Zsolt Kerner[c], Justyna Brasuń[d] Bartosz Setner[e] , Zbigniew Szewczuk[e] and Wiesław Malinka[b]

Received (in XXX, XXX) Xth XXXXXXXXX 20XX, Accepted Xth XXXXXXXXX 20XX
DOI: 10.1039/b000000x

Modifications in linear and cyclic peptides have been widely explored in relation with the associated effects on the coordination of Cu^{II}. Branching of peptides is yet another innovative conception to promote metal binding. The three dimensional (3D), quasi-tripodal structure of the new ligand, H-His-Dap(H-His)-His-NH_2 (3H, where Dap = *L*-2,3-diaminopropionic acid), which is created by the vicinal two N-terminal and one C-terminal function of Dap allows triple-arm extension and offers new options in metal binding. A strategy is presented for the characterization of 3H focusing on the role of structural domains in Cu^{II} binding by comparison of analogous tetrapeptides that involve a varying number of His and Gly residues. Potentiometric, spectroscopic (UV-Vis, CD and EPR), mass spectrometric and electrochemical data indicate that in monomeric Cu^{II}-3H complexes the metal is bound with higher affinity compared to its structural domains indicating that the effect of 3D branching should be taken as important factor for future studies on Cu^{II} peptide constructs.

Introduction

Applications of designed peptides as specific ligands for copper have become expansive, including catalysts/electrocatalysts [1], peptide based fluorescent metallo-probes[2], chelating agents in neurodegenerative diseases[3] and metal ion selective cell organelle targeting probes.[4] This advancement in applications was largely promoted by the decades-long studies on copper-peptide complexes triggered by their relevance to biological systems.[5] The number and position of certain residues in linear peptides, especially of histidine, substantially influences stability, coordination sphere and nuclearity of the complexes.[5,6]

Branching of peptides potentially improves the proteolytic and serum stability[7,8], selective cell uptake properties[9], and also, the metal binding efficiency.[10,3] The improved targeting properties of this peptide family, compared to linear ones, was applied in gene transport processes, e.g., His-rich peptides.[11] The unique, three dimensional (3D) structure was also improved to be more effective in multiple antigen peptides (MAP)[12] , in antibacterial[13] and in some therapeutic[14] agents. Expanding the field of new, triple-arm peptides and their metal complex engineering can be crucial for the further development of those applications as well as, new enzyme mimicking centers[15], some drugs[16], radiopharmaceutics[17] or novel artificial proteins.[18,19]

During the design of Cu-based biomimetics and bioinspired pharmaceuticals and in-cell metal transporters it is therefore desirable to consider the redox behavior of these systems. In addition, copper may occur in three oxidation states when ligated and usually one of the two possible single electron redox transitions, +3/+2 or +2/+1 between these states can be observed in copper enzymes and complexes with artificial ligands. This leads to rich redox chemistry[20] and catalysis, especially using molecular oxygen[21], and, in connection, the control of oxidative stress in living species.[22]

Peptide branching with lysine promotes formation of dimeric complexes.[3] In a recent study we demonstrated that dimerization at physiological pH can be suppressed with Dap-based branched peptides (Dap = *L*-2,3-diaminopropionic acid), H-Gly-Dap(H-Gly)-His-NH_2 (2GH) H-His-Dap(H-His)-Gly-NH_2 (2HG) (Fig. 1 2HG, 2GH).[10] Here we report a new branched tetrapeptide that is also built on Dap and contains one C-terminal and two N-terminal histidine residues (Fig. 1, 3H).

From our previous study we learnt that placement of one histidine residue at the C-, or two at the N-terminal of Dap influences the Cu^{II} binding mode very differently. Here we discuss how the simultaneous presence of both domains will affect Cu^{II} complex stabilization, paying special attention to redox properties which may be of crucial importance, since inside the living cells Cu^{I} can be often stabilized. During the design of Cu-based biomimetics and bioinspired pharmaceuticals and in-cell metal transporters it is therefore desirable to consider the redox behavior of these systems. In addition, copper may occur in

three oxidation states when ligated and usually one of the two possible single electron redox transitions, +3/+2 or +2/+1 between these states can be observed in copper enzymes and complexes with artificial ligands. This leads to rich redox chemistry[23] and catalysis, especially using molecular oxygen[21], and, in connection, the control of oxidative stress in living species.[22]

Electrochemical studies on copper complexes rarely go beyond cyclic voltammetry (CV) performed either in an aprotic solvent or in water at a fixed pH.[24–27] CV offers a wealth of experimental information and includes both kinetic and thermodynamic details of many chemical systems; on the other hand, pK_a values that substantially control short range proton transfer coupled to the electron transfer, and well defined formal potentials are only accessible when *E vs.* pH (Pourbaix) diagrams are considered.[20,23] For this reason, after the initial CV experiments we also applied square-wave voltammetry (SWV) to address the pH-dependence of the $Cu^{III/II}$ transition and fitted the data with a modified Nernst equation in part relying on the speciation and spectroscopic information.

Potentiometric, spectroscopic and mass spectrometry data indicate effect of N- and C-terminal cooperation in stabilization of Cu binding. Results from electrochemistry also underline the advantages of the simultaneous presence of histidine residues on each arm of three branched peptides.

Experimental

Ligand synthesis

Materials

All Fmoc amino acids, including Fmoc-L-Dap(Fmoc)-OH used as a branching amino acid, solvents and reagents were purchased from Iris Biotech GmbH (Marktredwitz, Germany) and used without further purification.

Peptide synthesis

The synthesis of the peptide H-His-Dap(H-His)-His-NH_2 was performed manually on the Rink Amide MBHA resin (loading: 0.52 mM/g) in a polypropylene syringe reactor (Intavis AG, Köln, Germany) equipped with polyethylene filter, according to the standard Fmoc (9-fluorenylmethoxycarbonyl) solid phase synthesis procedure. TBTU (*O*-(Benzotriazol-1-yl)-*N*,*N*,*N*',*N*'-tetramethyluronium tetrafluoroborate) was used as a coupling reagent (3 equivalents). Oxyma Pure (Ethyl 2-cyano-2-(hydroxyimino)acetate) (3 equivalents) and DIPEA (*N*,*N*-Diisopropylethylamine) (6 equivalents) were used as additives. DMF (*N*,*N*-Dimethylformamide) was used as solvent. Each coupling step was performed for 2h. After removal of the Fmoc-protecting groups, from the diaminopropionic acid derivative, attached to the resin, with 25% piperidine in DMF, a mixture of Fmoc-His(Trt)-OH/TBTU/Oxyma Pure/DIPEA (6 equivalents of each reagent) in DMF was added and stirred for 24h. The end of a coupling was confirmed by the Kaiser Test. The peptide was cleaved from the resin simultaneously with the side chain deprotection using a solution of TFA/H_2O/TIS (95/2.5/2.5, v/v/v) at room temperature for 2h and purified by semi-preparative RP-HPLC.

Purification and mass spectrometry analysis

The peptide was purified by the RP-HPLC using a Varian ProStar (Palo Alto, CA, California) with UV detection (210 nm and 280 nm) on a TSKgel ODS-120T 12TG08eh004 column (215 x 30.0 mm, 10 μm) equipped with a TSKguard column ODS (21,5x7.5 mm, 10 μm), with a gradient elution of 0-80% B in A (A = 0.1% TFA in water; B = 0.1% TFA in acetonitrile/H_2O, 4:1) for 40 min (flow rate 7 mL/min). The main peak, corresponding to the peptide H-His-Dap(H-His)-His-NH_2, was collected and the fraction was lyophilized. All spectrometric experiments for synthesis product identification were performed on a Bruker micrOTOF-Q mass spectrometer (Bruker Daltonics, Bremen, Germany) equipped with an ESI source. Analyte solutions (1 μg in 1 ml of 50:50 acetonitrile–water mixture containing 0.1% HCOOH) were pumped at a rate of 2 μL/min. The instrument was operated in the positive ion mode and calibrated before each analysis with the Tunemix™ mixture (Agilent Technologies, Santa Clara, USA) in quadratic method. For the MS spectra analysis, the Bruker Compass DataAnalysis 4.0 software was used. Sophisticated Numerical Annotation Procedure (SNAP) algorithm was used for finding peaks. The measured m/z for H-His-Dap(H-His)-His-NH_2 (3H) of $[M+H^+]$ ion was 515.2632 (calculated 515.2632).

Potentiometric studies

Peptide protonation and Cu^{II} complex stability constants were calculated from three titration curves carried out over the pH range 2.5 – 11.0 at 298 K under argon atmosphere. Ligand concentration was set in a range of 1×10^{-3} to 1.5×10^{-3} M. Metal-to-ligand ratio was 0.82 : 1, 0.85 : 1 and 0.95 : 1. The pH-metric titrations were performed in 0.1 M KCl on a Metrohm titrator using a Mettler Toledo InLab®Micro combined electrode calibrated for hydrogen ion concentration using HCl. The stability constants were calculated with HYPERQUAD 2013.[28] Standard deviations quoted were computed with the same software and refer to random errors only.

Spectroscopic studies (UV-Vis, CD, EPR)

Absorption spectra of Cu^{II} complexes were recorded on a PerkinElmer Lambda 25 spectrophotometer in 1 and 0.5 cm path length quartz cells. All UV-Vis spectra were collected in the 300-900 nm range. Circular dichroism (CD) spectra were recorded on a JASCO J 750 spectropolarimeter in the 250-900 nm range, using 1 and 0.1 cm cuvettes. Spectroscopic measurements were carried out at 298 K, at concentrations from 0.8 to 1.4×10^{-3} M and M : L = 1 : 1. Electron paramagnetic resonance (EPR) spectra were measured on a Bruker Elexsys 500 spectrometer operating at the X-band frequency (~9.7 GHz) at 123 K using narrow quartz capillaries to reduce the dielectric loss of the cavity. The ligand concentration was adjusted to $1\text{-}1.5\times10^{-3}$ M in 30% (v/v) polyethylene glycol/water solution. Data from X-Band EPR spectroscopy have been extracted by simulation of the experimental spectra taken at different pH values, at 123 K. For further details of the simulation method see ref.[10]

Mass spectrometry measurements

High-resolution mass spectra were obtained on a Bruker micrQ-FTMS spectrometer. Electrospray ionization (ESI-MS) mass spectra were measured in the positive ion mode. Before each run the instrument was calibrated externally with the Tunemix™

mixture. The ion source parameters were as follows: dry gas – nitrogen, temperature 170 °C, transfer time 120 ps, collision voltage -1.0 EV. The sample was dissolved in aqueous solution while the pH was adjusted with ammonium acetate to pH 4.5 and 6.8. The peptide concentration was in the 10^{-5} – 10^{-4} M range. The solution was infused at a flow rate of 3 µL/min. Simulations of the isotopic patterns were calculated using BrukerDataAnalysis 4.0 software.

Electrochemistry.

Cyclic voltammetry (CV), chronoamperometry (CA) and square-wave voltammetry (SWV) measurements were performed on a SP-150 potentiostat (BioLogic) equipped with a low-current unit. A standard three-electrode setup was used including a glassy carbon working electrode (GC, 0.072 cm^2), Pt auxiliary electrode (~2 cm^2) and Ag/AgCl (3 M KCl) reference electrode. The cell was modified to accommodate a pH microelectrode (Mettler-Toledo). The working electrode was carefully rinsed, polished and rinsed again right before each measurement (note that unpolished GC electrodes provide biased results, especially with peptides, for further information see refs.[29,30]. The cell was kept under argon throughout the measurements, the O_2 level was checked with an optical O_2 sensor (Ocean Optics NeoFox). SWV settings were: 0.73 mM Cu-3H, 100 mM $NaClO_4$ electrolyte, 25 °C, pulse width 10 ms (f = 50 Hz), step potential 0.2 mV, SW pulse height 25 mV. The raw current curves (net current, I_{net} = forward minus reverse current, I_{for}-I_{rev}) were baseline corrected uniformally with fitted cubic baselines to obtain the curves plotted in Fig. 7. All salts were purchased from commercial sources and were of puriss p.a. grade.

Results and discussion

Potentiometric titration, ESI-MS and pH-dependence of UV-Vis, CD and EPR spectroscopy

Complex formation between 3H and Cu^{II} in a ~1:1 solution starts already at acidic pH and increasing the pH to 3.5 results in a dominant CuH_3L complex (Fig. 2, Table 1). The observed UV-Vis parameters for this species are close to those where Cu^{II} is bound with $\{2N_{im}\}$ donors.[31] This finding is in good agreement with analysis of potentiometric data, since the $\log K^*_{CuL}$ = $\log\beta_{CuH3L} - \log\beta_{H3L}$ = 6.21(1) is close to $\log K^*_{CuL}$ of complexes with $\{2N_{im}\}$ proposed in the literature ($\log\beta^*$ = 6.4[32] or 6.48[31]).

X-Band EPR spectroscopic results (Table 2, Fig. 3) support this speciation, indicating the presence of two additional species to Cu^{II}_{aq} up to pH ~4.5 (Fig. 2). It is apparent from the experimental X-band EPR spectra that these S = 1/2 species give axial signal with $g_{||} > g_{\perp} > 2.0$, but lower than g-values for Cu^{II}_{aq}. The characteristic $A_{||}^{Cu} >> A_{\perp}^{Cu}$ splitting pattern is typical for d_{x2-y2} ground state.[33] More precise g-tensors, hyperfine (hf) and superhyperfine (shf) coupling parameters were extracted by simulation of the spectra. The simulated component spectra for the contributing species at a given pH were fitted by optimalization of the typical couplings of the unpaired electron to the ^{63}Cu and ^{65}Cu nuclei (I = 3/2). Shf coupling to nitrogen nuclei (^{14}N, I = 1) can be expected for the copper-peptide complexes. Although the shf couplings to different numbers of equal nitrogen nuclei (Table 2) in the equatorial positions at lower pH remain unresolved, they still contribute to the improvement of the fittings. Rhombic anisotropy, *e.g.*, splitting of $g_{||}$ to g_x and g_y, at a varying level occurs in the investigated pH range (from 3 to 10) indicating distortion of the elongated octahedral (or square-based pyramid) geometry. In particular, the EPR parameters for CuH_3L corroborate other spectroscopic results. In the pH range 4.5-5.8 the CuHL and CuL species dominate (Fig. 2). The switch between the 2GH and 2HG domains (Fig. 1), more specifically the histidine at the C-terminal arm of 2GH starts to play critical role in Cu^{II} binding when pH is increased (Fig. 4, Fig. S1).

Table 1. The logarithms of the protonation constants ($\log\beta_{HxL}$) and stability constants ($\log\beta_{CuhL}$) for Cu^{II} complexes with 3H, UV-Vis and CD spectroscopic parameters data for the respective species (T = 298 K, I = 0.1 M KCl).

Species	Potentiometry		UV-VIS	CD
	Logβ	log$K$	(λ [nm], ε [$M^{-1}cm^{-1}$])	(λ [nm], $\Delta\varepsilon$ [$M^{-1}cm^{-1}$])
H_5L	30.69(3)	4.47(2)		
H_4L	26.22(3)	5.28(2)		
H_3L	20.94(3)	6.17(2)		
H_2L	14.77(2)	6.99(2)		
HL	7.78(3)			
CuH_3L	27.16(1)		670, 29	
CuHL	19.51(1)	5.28(2)	538, 60	562, -0.37 487, 0.15 311, 0.45 272, sh
CuL	14.23(3)	6.29(2)	532, 91	562, -0.60 478, 0.21 311, 0.97 272, sh
$CuH_{-1}L$	7.95(3)	7.51(3)	530, 98	563, -0.61 478, 0.22 308, 1.23 271, sh
$CuH_{-2}L$	0.43(4)		528, 103	561, -0.64 480, 0.23 309, 1.24 271, sh

The ESI-MS results carried out at pH 6.8 confirmed the exclusive occurrence of monomeric complex in case of Cu : L molar ratios of 0.4 : 1.0 and 0.7 : 1.0. The observed Cu - L signal pattern corresponds to a two single charged ions with the molecular formula $Cu^{II}[C_{21}H_{29}N_{12}O_4]^+$ and $Cu^{I}[C_{21}H_{30}N_{12}O_4]^+$, which is in agreement with the formation of a 1 : 1 Cu – 3H complex. Also, the linear increase in absorption near 529 nm support occurrence of equimolar complexes in the range of Cu^{II} equivalent from 0 -1 (Fig. S2).

The UV-Vis absorption maximum (Cu d-d transition) shifts from 670 nm (associated with CuH_3L) to 538 and 532 nm associated with the CuHL and CuL, respectively (Table 1). This observation supports that in CuHL and CuL the metal ion is bound in 4N equatorial donor sets.[34] This is in agreement with the EPR

spectroscopy parameters which indicate 4 nitrogen donors in the equatorial plane (Table 2, Fig. 3). The logK correlated to the change of CuHL to CuL is 5.28(2). This observation as well as a shift in Δε near 311 nm in the CD spectra suggest the involvement of an amide donor in the CuL complex, in addition, the EPR and UV-Vis data indicate that both species, CuHL and CuL have 4 nitrogen donor set with a very similar ligand field.

Based on the known Cu-peptide complex structures at pH 4.5-5.8 with linear[5,6] and cyclic peptides[35] it could be proposed that in 3H at least eight nitrogen donors arranged in a three dimensional net are available for Cu^{II} binding, including 5 and 6 member chelate forming sites (Fig. S1a). This allows for exchange of nitrogen donors as pH changes. In order to understand the potential role of structural motifs in metal binding the partial structural analogs to 3H were used in further comparisons (Fig. S1bcd).

Table 2 . EPR parameters for the pH-dependent Cu-3H species and Cu^{II}.[a]

	Cu^{2+}	CuH_3L	"CuHL+CuL"[b]	$CuH_{-1}L$	$CuH_{-2}L$
$g_{\|\|}$ (g_z)	2.417	2.3010	2.1948	2.1865	2.1906
$g_\perp$ (g_x, g_y)	2.0826	2.0569, 2.0726	2.0407, 2.0544	2.0387, 2.0536	2.0407, 2.0511
$A^{Cu}_{\|\|}$ (A^{Cu}_z)	129	168	193	198	196
$A^{Cu}_\perp$ (A^{Cu}_x, A^{Cu}_y)	4	7, 8	9, 17	11, 21	14, 27
$a^N_{\|\|}$[c]	-	8 (2N)	8 (4N)	8 (4N)	8 (4N)
$a^N_\perp$ (a^N_x, a^N_y)	-	11, 9 (2N)	11, 12 (4N)	14, 15 (4N)	11, 14 (4N)

[a] $[|A|] = 10^{-4}cm^{-1}$.
[b] CuHL and CuL were considered with the same parameters
[c] estimation from unresolved structures (the effect is comparable to line broadening)

The 2HG peptide (Fig. S1b), which contains Gly instead the C-terminal His residue of 3H, in the 4.5-5.5 pH range binds Cu^{II} by its N-terminal fork.[10] The UV-Vis (λ/ε = 620/100) and CD (λ/Δε = 668/074, 321/–0.41) spectroscopic parameters for 2HG supported a 3N complex. The data for CuHL (L = 3H) in the same pH range are very different and consistent with a 4N environment (Tables 1 and 2). This difference excludes the option of closely related metal coordination by 2HG and 3H in this pH range (Fig. S1b).

The H-HVH-OH peptide represents the backbone peptide chain of 3H (Fig. S1c). The spectroscopic parameters for the corresponding Cu^{II} complexes with H-HVH-OH and 3H are also incompatible. In case of H-HVH-OH at pH 4.5-5.5 two complexes, CuHL and CuL (L = H-HVH-OH) were observed. The UV-Vis (λ/ε) parameters, 690/26 and 630/46, support 3N and 4N complexes, respectively[36] and are different from those observed for CuHL (L = 3H). The difference between the above listed data negates the hypothesis that the N- and C- terminal backbone arms of 3H (Fig. S1c) are unaccompanied in the binding of Cu^{II} in this pH region.

Finally, for 2GH, in which both N-terminals are Gly residues, instead of the His residues for 3H (Fig. S1d), the UV-Vis parameters, (λ/ε) 529/98, in the respective pH range were assigned to $CuH_{-1}L$. In this complex the $\{NH_2, 2N^-, N_{im}\}$ donor set is expected.[10] The differences in (λ/ε) 538/65 from CuHL (L = 3H) don't support hypothesis about exactly the same coordination mode, however, strong similarity is observed in the CD spectra corresponding to CuL indicating the special role of the C-terminal arm. (For 2GH the respective data are (λ/Δε) 568/–0.58, 481/0.23, 305/1.28 and 270/–2.05). This close resemblance indicates structural similarities between Cu-2GH and Cu-3H in this pH region.[37]

Based on the presented information we conclude that even the presence of two N-terminal His arms in 3H peptide is insufficient to force out the C-terminal His from the coordination sphere of Cu^{II}. It follows that the C-terminal localization of His is strongly desirable for Cu^{II} binding already at slightly acidic pH.

As a summary, it can be proposed that all three arms should participate in Cu^{II} coordination either by direct metal ligation or by the support of a hydrogen bond network causing very little spectroscopic differences between the CuHL and CuL.[38,39]

Formation of $CuH_{-1}L$ (Fig. 2 pH 6-7) is accompanied by moderate changes in UV-Vis, CD and also EPR spectroscopy (Tables 1 and 2). The spectroscopic parameters are closely related to the Cu^{II} complex with 2GH which occurs in this pH range and in which the metal is bound by $\{NH_2, 2N^-, N_{im}\}$.[10] This close similarity in the spectroscopic parameters indicates that 3H at pH 7 binds the Cu^{II} with the involvement of the C- and N- terminal main chain arms.

Interestingly, CuHL, CuL and $CuH_{-1}L$ dominate in the pH range 4.5 -7 where the switching between the affinity for Cu^{II} binding was calculated based on the stability constants (Fig. 4) and was also proved experimentally.[10] Forming of these intermediate forms with spectroscopic parameters between those known for 2HG at low pH and 2GH at high pH is justified by switching of Cu^{II} binding between the corresponding branched peptide arms in 3H.

Further increase in pH up to 9 results in $CuH_{-2}L$ (L = 3H). This process with logK = 7.51(3) does not induce significant spectroscopic changes and could be rationalized by the deprotonation of the non-coordinated amino group at one of the N-terminal branches, but nowise with any major changes in the first coordination sphere $CuH_{-2}L$.

Competition study between Dap-based peptides

Fig. 6 shows the distribution of Cu^{II} among 2GH, 2HG and 3H, present in equal concentration. First of all, the Cu^{II} distribution switches between 2HG and 2GH (Fig. 6ac) near pH 6. Up to pH 5 2HG, while above pH 7 the 2GH is the

predominant ligand. Between pH 5 and 7 both peptides were found to be competitive (Fig. 6b).[10] Somewhat surprisingly 3H is by far the best Cu^{II} complexing agent in the whole pH range, leaving behind both its N- (2HG) and C- terminal (2GH) domains (Fig. 1, S1bd). The coordination profile observed in case of 3H in the pH range up to 3.5 can be recognized as similar to 2HG (Fig. 1a), above pH 7 as similar to 2GH (Fig. 1b). In the region between 3.5 and 7 the involvement of all three branches in complexation of Cu^{II} is proposed. The observed extra stabilization may be rationalized by means of hydrogen bond network, similar to those observed for long, linear multi-histidine tags and histidine rich proteins.[38,39]

Electrochemistry

The cyclic voltammograms (CVs) of the Cu-3H system were recorded at pH 7 and 8 (Fig. 7). This pH region is common condition for many of the enzymatic processes and biological environments. Under the given conditions 3H has high affinity for Cu^{II} (Fig. 6), but the question of redox stability remains open. Cathodic polarization of the GC working electrode yields a Faradaic current peak that shifts to more negative potential by ~40 mV with increasing pH to 8 (E_{pc1}'). On the reverse direction the anodic current peak occurs at considerably higher potential (E_{pa1}') that is clear indication of a rapid background chemical process (electrochemical-chemical-electrochemical, ECE mechanism).

Such behavior is often observed for $Cu^{II/I}$ transitions as the change in the redox state induces fundamental changes in the coordination number and geometry.[40] In the pH range of 6-8, Cu-3H complexes are present in three protonation states: $Cu^{II}L$, (and predominantly) $Cu^{II}H_{-1}L$ and $Cu^{II}H_{-2}L$ (Fig. 2). The pH-dependent spectroscopic features indicate (*vide supra*) that the coordination sphere - involving all three arms and consisting of 3 neutral N donor groups beside one N^- - transforms to $\{NH_2,2N^-,N_{im}\}$ upon deprotonation of $Cu^{II}L$. Hureau *et al.* compared the redox features of $[Cu^{II}(GHK)]$ (with $1N_{im}$), $[Cu^{II}(GHK)_2]$ (with $2N_{im}$) and $[Cu^{II}(GHK)(His)]$ (with $2N_{im}$) (GHK = H-Gly-His-Lys-OH) at pH = 7.4 and suggested that addition of N_{im} will prevent losing the metal upon reduction[41], which otherwise leads to metallic copper deposition at the electrode. As a characteristic feature in CV they observed in the anodic direction a Cu^0 to Cu^I oxidation-solubilization current peak beside the Cu^I to Cu^{II} peak.

All this information led us to propose a mechanism (Scheme 1) for the observed $Cu^{II/I}$ redox cycle of the Cu-3H system. According to this mechanism, the irreversible, pH-dependent E_{pc1}' can be assigned as the $Cu^{II}H_{-1}L$ to $Cu^{I}L$ proton coupled electron transfer (PCET) reaction, while the E_{pa1}' to the $Cu^{I}L$ to $Cu^{II}L$ oxidation. The driving force of this mechanism is the possibility of intra-ligand translocation of copper upon reduction, allowed by the branched structure of 3H. Once in the CuL form, the changed donor set will accommodate both Cu^I and Cu^{II}. One may suppose as an alternative assignment for E_{pc1}' that $Cu^{II}H_{-1}L$ is reduced directly to $Cu^{I}H_{-1}L$. This species would most likely release Cu^I, or may again translocate Cu^I to the available His arms. The presence of free Cu^I would lead to oxidation-solubilization current peak, but this is not observed in the presented voltammograms. Therefore we suggest that, if free Cu^I is produced at all, it will be rapidly re-complexed by the neutral free ligand according to Scheme 1. The Cu-3H system exhibits a quasi-reversible $Cu^{III/II}$ redox transition at pH 6.98 (Fig. 7, E_{pa2}' and E_{pc2}') with $E_{1/2}$ ~ 0.88 V *vs.* Ag/AgCl, ΔE_p ~ 100 mV and approximating $I_a = I_c$ at 200 mV/s. Chronoamperometry indicates that the current peaks associated with the $Cu^{II/I}$ and $Cu^{III/II}$ processes involve equal number of electrons (Fig. S3). The $E_{1/2}$ value in comparison with literature examples where the equatorial binding plane of the complex is reported[41,40,42,1], suggests a $\{NH_2,2N^-,N_{im}\}$ donor plane that is exactly what spectroscopic results indicate for $Cu^{II}H_{-1}L$ and $Cu^{II}H_{-2}L$. However, when the pH is shifted to 8, even at 400 mV/s, I_a considerably exceeds I_c, showing that an EC_{rev} mechanism is operating accelerated by basic pH and competing with the electrochemical reduction of Cu^{III} on the CV timescale. A decrease in the peak potentials of ~30 mV could be estimated.

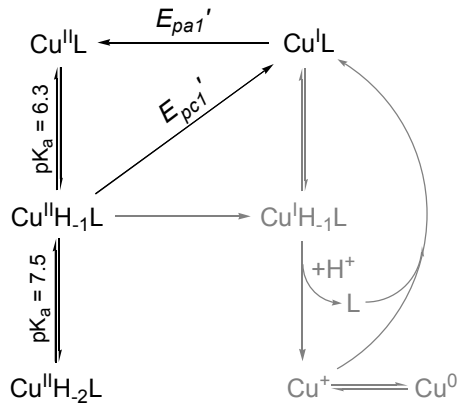

Scheme 1. Proposed processes that contribute to the observed $Cu^{II/I}$ redox transitions in the CVs.

To our knowledge, information on the pH-dependence of $Cu^{III/II}$ transitions in Cu-peptide complexes is rare in literature[23,43], despite that proton transfer processes coupled to redox transitions (PCET) are of key importance in biochemistry and catalysis.[44] Therefore we aimed to determine the $Cu^{III/II}$ potential in the pH range from 7 to 8.8 for the Cu-3H system. In this range the $Cu^{II}H_{-1}L$ and $Cu^{II}H_{-2}L$ forms are predominant. Instead of CV we applied square-wave voltammetry (SWV) to determine the $E°'$ values accurately, upon shifting the pH by small increments.[1] The E_{net} (potential of I_{net}) vs. pH plots will directly give Pourbaix diagrams, when reversibility terms of the electrode process are fulfilled. Figure 8 summarizes the SWV results for the $Cu^{III/II}$ transition (Table S1 sums the data, Fig. S4 illustrates reproducibility). In Fig. 8a the E_{net} data points are plotted against the pH generating a Pourbaix diagram for the $Cu^{III/II}$ process. Note that the I_{for}/I_{rev} ratio approximating 1 (Fig. 8c) and symmetrical current peaks are landmarks of reversibility on the timescale of the experiment. Presuming that eq. (1) describes the electrochemical process, a modified Nernst equation (2) can be written to explain the pH-dependence of E_{net}.[45] In this equation we presume the involvement of both the reduced (Cu^{II}) and oxidized (Cu^{III}) form in one protic equilibrium:

$$Cu^{III}H_{-2}L + e^- \rightleftharpoons Cu^{II}H_{-2}L \qquad (1)$$

$$E_{net} = E°'(Cu^{III}H_{-2}L/Cu^{II}H_{-2}L,\ pH = 0) + \\ + 0.0591 \log \frac{K_a(red) + [H^+]}{K_a(red)K_a(ox) + K_a(red)[H^+]} - 0.0591pH \quad (2)$$

where $K_a(red)$ is the acid dissociation constant of $Cu^{II}H_{-1}L$ to $Cu^{II}H_{-2}L$, $K_a(ox)$ is the acid dissociation constant of $Cu^{III}H_{-2}L$ to $Cu^{III}H_{-3}L$ and $E°'$ ($Cu^{III}H_{-2}L/Cu^{II}H_{-2}L$, pH = 0) is the formal potential of the process in eq. (1). Fit of eq. (2) to E_{net} data points yields the line in Fig. 8a and parameters as listed in Table 3.

Table 3. Formal potential and pK_a values derived from the fit of eq. (2) to experimental E_{net} *vs.* pH data for the $Cu^{III/II}$ redox transition

	eq. (2)
p$K_a(red)$	7.3(1)
$E°'$ ($Cu^{III}H_{-2}L/Cu^{II}H_{-2}L$) *vs.* Ag/AgCl (V)	0.831(3)
p$K_a(ox)$	8.7(1)

The p$K_a(red)$ is in satisfactory agreement with the logK = 7.51(3) value for the $Cu^{II}H_{-1}L$ form derived from potentiometry. The projections of the fitted function to pH = 0 (*e.g.*, $E°'(Cu^{III}H_{-2}L/Cu^{II}H_{-2}L,\ pH = 0) + 0.0591pK_a(red\ or\ ox)$) give $E°'(Cu^{III}H_{-2}L,H^+/Cu^{II}H_{-1}L,\ pH = 0)$ as 1.26 V and $E°'(Cu^{III}H_{-3}L,H^+/Cu^{II}H_{-2}L,\ pH = 0)$ as 1.34 V. These potentials along with the fit parameters can be assigned to equilibria, which are arranged into a stepladder scheme of the PCET processes (Scheme 2, protons and electrons are omitted for sake of simplicity).

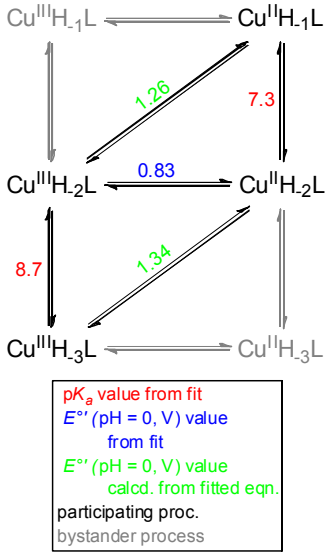

Scheme 2. Processes operating in the pH range of the SWV study.

The horizontal equilibria involve no change in protons (ET), while vertical ones no change in electrons (PT). The diagonal processes are assigned as multiple site electron-proton transfer (MS-EPT[44]) processes, differing in their potential by 0.0591pK_a (red or ox) from the value for the ET of 0.83 V. According to this scheme, the MS-EPT processes become favored for the Cu-3H system at pH below p$K_a(red)$ and above p$K_a(ox)$.

Conclusions

Our strategy to combine in one three dimensional branched peptide two structural motifs with maximal Cu^{II} binding efficiency in different ranges of pH, resulted in the design of the novel triple-arm peptide 3H. Our data demonstrate that structure can significantly increase Cu^{II} binding affinity. The extra stabilization of Cu-3H complexes in comparison with analogues of the Cu^{II} binding domains indicate that all arms are involved in metal binding near the physiological pH, moreover, the C-terminal His residue is dominating.

Prolongation of the the C-terminal peptide arm therefore can be recommended in order to functionalize the complex with, for example, anchoring moiety or peptide sequence targeting. Importantly, upon reduction of Cu^{II} to Cu^{I} bound to 3H no metal deposition was observed at the electrode, indicating that the ligand can retain Cu^{I} from dissociation. We attribute this behavior to the propensity of 3H to flexibly adopt its structure to altered redox conditions. This advantage of 3H is also traced in supporting a $Cu^{III/II}$ redox transition among the very same conditions, separated by ~1.2 V from the Cu^{II} to Cu^{I} reduction. Our electrochemical investigations suggest that PCET processes play key role in redox-coupled structure switching. Surface anchoring of our complexes will be explored in upcoming studies.

This experience can be applied in the design of Cu^{II}- peptide based radiopharmaceuticals, metal sensors, peptide based Cu^{II} fluoroprobes and also applied in the catalytic/electocatalytic multi histidine metallopeptides or artificial proteins. The presented Dap peptide frame and branching methodology may help achieve the desirable goal of elucidating the contribution of different aminoacids (donor groups) localized in different positions of three dimensional net to understand their role in copper biding and activity.

Acknowledgements.

This study was supported by a Polish Foundation of Science within the POMOST program co-financed by the European Union within European Regional Development Fund (POMOST/2012-5/9). Support from the MTA through a János Bolyai Scholarship is also acknowledged (J. S. Pap).

Notes and references

[a]CNRS/UPPA, LCABIE, UMR5254, Helioparc, 2, av. Pr. Angot, F-64053 Pau, France. Fax: 33-5594-07681; Tel: 33-5594-07739; E-mail: lukasz.szyrwiel@univ-pau.fr
[b]Department of Chemistry of Drugs, Wrocław Medical University, ul. Borowska 211, 50-552 Wrocław, Poland.
[c]MTA Centre for Energy Research, Surface Chemistry and Catalysis Department, PO Box 49, H-1525 Budapest, Hungary.
[d]Department of Inorganic Chemistry, Wroclaw Medical University, Borowska 211a, 50-552 Wroclaw, Poland.
[e]Faculty of Chemistry, University of Wrocław, ul. F. Joliot-Curie 14, 50−383 Wrocław, Poland.

† Electronic Supplementary Information (ESI) available: Figs. S1-S4, Table S1. See DOI: 10.1039/b000000x/

1. J. S. Pap, L. Szyrwiel, D. Sranko, Z. Kerner, B. Setner, Z. Szewczuk, and W. Malinka, *Chemical Communications*, 2015.
2. T. R. Young, C. J. K. Wijekoon, B. Spyrou, P. S. Donnelly, A. G. Wedd, and Z. Xiao, *Metallomics*, 2015, **7**, 567–578.
3. A. Lakatos, B. Gyurcsik, N. V Nagy, Z. Csendes, E. Wéber, L. Fülöp, and T. Kiss, *Dalton transactions (Cambridge, England : 2003)*, 2012, **41**, 1713–26.
4. L. Szyrwiel, M. Shimura, J. Shirataki, S. Matsuyama, A. Matsunaga, B. Setner, L. Szczukowski, Z. Szewczuk, K. Yamauchi, W. Malinka, L. Chavatte, and R. Lobinski, *Metallomics*, 2015.
5. H. Kozłowski, W. Bal, M. Dyba, and T. Kowalik-Jankowska, *Coordination Chemistry Reviews*, 1999, **184**, 319–346.
6. I. Sóvágó, C. Kállay, and K. Várnagy, *Coordination Chemistry Reviews*, 2012, **256**, 2225–2233.
7. C. Falciani, L. Lozzi, A. Pini, F. Corti, M. Fabbrini, A. Bernini, B. Lelli, N. Niccolai, and L. Bracci, *Chemical Biology & Drug Design*, 2007, **69**, 216–221.
8. L. Bracci, C. Falciani, B. Lelli, L. Lozzi, Y. Runci, A. Pini, M. G. De Montis, A. Tagliamonte, and P. Neri, *Journal of Biological Chemistry* , 2003, **278** , 46590–46595.
9. G. A. Eggimann, S. Buschor, T. Darbre, and J.-L. Reymond, *Organic & Biomolecular Chemistry*, 2013, **11**, 6717–6733.
10. Ł. Szyrwiel, Ł. Szczukowski, J. S. Pap, B. Setner, Z. Szewczuk, and W. Malinka, *Inorganic Chemistry*, 2014, **53**, 7951–7959.
11. Q. Leng and A. J. Mixson, *Nucleic Acids Research* , 2005, **33** , e40.
12. K. Sadler and J. P. Tam, *Reviews in Molecular Biotechnology*, 2002, **90**, 195–229.
13. M. Stach, N. Maillard, R. U. Kadam, D. Kalbermatter, M. Meury, M. G. P. Page, D. Fotiadis, T. Darbre, and J.-L. Reymond, *MedChemComm*, 2012, **3**, 86–89.
14. S. P. Liu, L. Zhou, R. Lakshminarayanan, and R. W. Beuerman, *International journal of peptide research and therapeutics*, 2010, **16**, 199–213.
15. A. Esposito, E. Delort, D. Lagnoux, F. Djojo, and J.-L. Reymond, *Angewandte Chemie International Edition*, 2003, **42**, 1381–1383.
16. J. E. Wynn and W. L. Santos, *Organic & Biomolecular Chemistry*, 2015, **13**, 5848–5858.
17. J. L. Hickey, E. J. Simpson, J. Hou, and L. G. Luyt, *Chemistry – A European Journal*, 2015, **21**, 568–578.
18. T. Darbre and J.-L. Reymond, *Accounts of chemical research*, 2006, **39**, 925–34.
19. A. G. Tebo and V. L. Pecoraro, *Current Opinion in Chemical Biology*, 2015, **25**, 65–70.
20. D. B. Rorabacher, *Chemical Reviews*, 2004, **104**, 651–698.
21. K. D. Karlin, *Wiley, Hoboken-New Jersey, 2011*, 2011.
22. H. Kozlowski, A. Janicka-Klos, J. Brasun, E. Gaggelli, D. Valensin, and G. Valensin, *Coordination Chemistry Reviews*, 2009, **253**, 2665–2685.
23. M. R. McDonald, F. C. Fredericks, and D. W. Margerum, *Inorganic Chemistry*, 1997, **36**, 3119–3124.
24. P. Faller, C. Hureau, P. Dorlet, P. Hellwig, Y. Coppel, F. Collin, and B. Alies, *Coordination Chemistry Reviews*, 2012, **256**, 2381–2396.
25. K. P. Neupane, A. R. Aldous, and J. A. Kritzer, *Journal of Inorganic Biochemistry*, 2014, **139**, 65–76.
26. C. Hureau, H. Eury, R. Guillot, C. Bijani, S. Sayen, P.-L. Solari, E. Guillon, P. Faller, and P. Dorlet, *Chemistry – A European Journal*, 2011, **17**, 10151–10160.
27. A. B. Grosas, P. Kalimuthu, A. C. Smith, P. A. Williams, T. J. Millar, P. V Bernhardt, and C. E. Jones, *Neurochemistry International*, 2014, **70**, 1–9.
28. P. Gans, A. Sabatini, and A. Vacca, *Talanta*, 1996, **43**, 1739–1753.
29. B. W. Berry, M. C. Martínez-Rivera, and C. Tommos, *Proceedings of the National Academy of Sciences* , 2012, **109** , 9739–9743.
30. Ed. F. Scholz, *Springer-Verlag, Berlin*, 2010.
31. C. Kállay, K. Várnagy, G. Malandrinos, N. Hadjiliadis, D. Sanna, and I. Sóvágó, *Inorganica Chimica Acta*, 2009, **362**, 935–945.
32. A. Matera-Witkiewicz, J. Brasuń, J. Świątek-Kozłowska, A. Pratesi, M. Ginanneschi, and L. Messori, *Journal of Inorganic Biochemistry*, 2009, **103**, 678–688.
33. B. J. Hathaway, G. Wilkinson, R. D. Gillard, and J. A. McCleverty, *Comprehensive Coordination Chemistry*, 1987, **5**, 533–774.
34. E. Prenesti, P. G. Daniele, S. Berto, and S. Toso, *Polyhedron*, 2006, **25**, 2815–2823.
35. J. Brasun, C. Gabbiani, M. Ginanneschi, L. Messori, M. Orfei, and J. Swiatek-Kozlowska, *Journal of Inorganic Biochemistry*, 2004, **98**, 2016–2021.
36. a Myari, G. Malandrinos, Y. Deligiannakis, J. C. Plakatouras, N. Hadjiliadis, Z. Nagy, and I. Sòvágó, *Journal of inorganic biochemistry*, 2001, **85**, 253–61.
37. H. F. Stanyon, X. Cong, Y. Chen, N. Shahidullah, G. Rossetti, J. Dreyer, G. Papamokos, P. Carloni, and J. H. Viles, *FEBS Journal*, 2014, **281**, 3945–3954.
38. A. Jancsó, A. Kolozsi, B. Gyurcsik, N. V Nagy, and T. Gajda, *Journal of Inorganic Biochemistry*, 2009, **103**, 1634–1643.
39. J. Watly, E. Simonovsky, R. Wieczorek, N. Barbosa, Y. Miller, and H. Kozlowski, *Inorganic Chemistry*, 2014, **53**, 6675–6683.
40. C.-T. Lin, D. B. Rorabacher, G. R. Cayley, and D. W. Margerum, *Inorganic Chemistry*, 1975, **14**, 919–925.
41. B. Alies, B. Badei, P. Faller, and C. Hureau, *Chemistry – A European Journal*, 2012, **18**, 1161–1167.
42. C. Hureau, L. Charlet, P. Dorlet, F. Gonnet, L. Spadini, E. Anxolabéhère-Mallart, and J.-J. Girerd, *JBIC Journal of Biological Inorganic Chemistry*, 2006, **11**, 735–744.
43. M.-T. Zhang, Z. Chen, P. Kang, and T. J. Meyer, *Journal of the American Chemical Society*, 2013, **135**, 2048–2051.
44. D. R. Weinberg, C. J. Gagliardi, J. F. Hull, C. F. Murphy, C. A. Kent, B. C. Westlake, A. Paul, D. H. Ess, D. G. McCafferty, and T. J. Meyer, *Chemical Reviews*, 2012, **112**, 4016–4093.
45. P. Wardman, *J. Phys. Chem. Ref. Data*, 1989, **18**, 1637–1755.

{Bibliography}

Figure captions

Figure 1. Graphical presentation of combining two 2,3-diaminopropionic branched peptides in one that contains both metal binding histidine domains. The two N-terminals peptide arms are marked with red and the C-terminal arm is marked with blue. 2HG = H-His-Dap(H-His)-Gly-NH_2, 2GH = H-Gly-Dap(H-Gly)-His-NH_2 and 3H = H-His-Dap(H-His)-His-NH_2 peptides.

Figure 2. Speciation diagram for the system containing Cu^{II} and 3H, $[Cu^{II}] = 1 \times 10^{-3}$ M, $1Cu^{II} : 1L$ (where L = 3H).

Figure 3. Experimental (red) and simulated (black) EPR spectra at different pH for the Cu^{II} : 3H system.

Figure 4. Speciation diagram for Cu^{II} and 3H, dashed lines show curves of competition for Cu^{II} between the ligands 2HG (red), 2GH (blue). The gray rectangle illustrates the region where the switching between branches that participate in Cu^{II} binding takes place as the respective complex species marked with green (CuHL, CuL and $CuH_{-1}L$) occur (the conditions of speciation and competition diagram: $[Cu^{II}] = [3H] = 1\times10^{-3}$ M, $[Cu^{II}] = [2GH] = [2HG] = 1 \times 10^{-3}$ M respectively).

Figure 5. The (+)ESI-MS spectrum of the Cu^{II} – L mixture at pH 6.8: (a) the Cu^{2+}: L ratio was 0.4 : 1.0 and (b) the Cu^{2+}: L ratio was 0.7 : 1.0 ($C_L = 0.8 \times 10^{-4}$ M, where L = 3H). Respective, blown up regions of spectra are marked with red and blue.

Figure 6. Competition plot showing the distribution of Cu^{II} between 2GH, 2HG and 3H as a function of pH, $[Cu^{II}] = [2GH] = [2HG] = [3H] = 1\times10^{-3}$ M. Partitions denote those pH regions where spectroscopic parameters of 3H could be recognized as: a) similar to 2HG (red), b) 3H specific (2HG and 2GH competitive region), c) similar to 2HG (blue).

Figure 7. Cyclic voltammograms of the Cu-3H system (2 mM in water, 0.1 M $NaClO_4$, under argon at 25°C) at pH 7.0 (bottom) and at pH 8.0 (top) plotted on the same scale. The initial potential is 0.6 V for scans to both the anodic and cathodic directions (see blue and brown arrowheads).

Figure 8. (a) $Cu^{III/II}$ net potentials (E_{net}) determined by square-wave voltammetry (SWV) and plotted as a function of pH. The solid line represents a nonlinear regression curve fit to eq. (2) ($R^2 = 0.9857$, for parameters see Table 3). (b) Baseline corrected net current SW voltammograms of the Cu-3H system between pH 7.04 and 8.79. The potentials in Fig. 7a correspond to E_{net} of the baseline corrected net current traces, $I_{net} = I_{for} - I_{rev}$, where forward means the current response to the oxidation pulse while reverse to the reduction pulse. (c) Plot of the ratio of I_{for} and I_{rev} components as a function of pH. SWV conditions: 0.7 mM Cu-3H, 100 mM $NaClO_4$, temperature 25.0±0.1 °C, tp = 10 ms (f = 50 Hz), step potential 0.2 mV, SW pulse amplitude 25 mV, 0.072 cm^2 GC working electrode, ~2 cm^2 Pt auxiliary electrode and Ag/AgCl (3 M KCl) reference electrode. All experiments were conducted under an Ar blanketing atmosphere, where O_2 concentration was < 2 μM.

Table 1. The logarithms of the protonation constants ($\log\beta_{HxL}$) and stability constants ($\log\beta_{CuhL}$) for Cu^{II} complexes with 3H, UV-Vis and CD spectroscopic parameters data for the respective species (T = 298 K, I = 0.1 M KCl).

Table 2 . EPR parameters for the pH-dependent Cu-3H species and Cu^{II}.

Table 3. Formal potential and pK_a values derived from the fit of eq. (2) to experimental E_{net} *vs*. pH data for the $Cu^{III/II}$ redox transition.

Supplementary figure captions

Figure S1. A) the molecular scheme showing possible interactions (marked with doted line) between 3H and Cu^{II} including 5 and 6 member chelate rings. Schematic presentation of ligands known from literature (column I), respective domains of 3H peptide (column II) and their impact in the possible metal binding within the 3H peptide (column III); a) 2HG (H-His-Dap(H-His)-Gly-NH_2), b) H-HVH-OH (H-His-Val-His-OH), (c 2GH (H-Gly-Dap(H-Gly)-His-NH_2).

Figure S2. The UV-vis spectra showing the titration of 3H with Cu^{2+} at physiological pH (7.4) from 0.0 : 1.0 up to 2.0: 1.0 ratio (Cu^{II} : L).

Figure S3. Chronoamperometry (CA) plot showing a forward and reverse sequence of three potentials (1.0, 0.4 and -0.4 V vs. Ag/AgCl) set consecutively to the GC working electrode for 5 seconds. Data indicate that the observed oxidation and reduction (assigned as the $Cu^{III/II}$ and $Cu^{II/I}$ redox transitions) involve equal number of electrons. Conditions are identical to those of CV scans at pH 6.98.

Figure S4. Background-corrected SWVs showing the $Cu^{III/II}$ response for Cu-3H at pH = 7.51(7.55) obtained from two independent measurements on two different samples using identical experimental settings. The average error in the current peak potential value is ~4 mV.

Table S1. Formal potentials derived from SWV for the $Cu^{III/II}$ redox transition of the Cu-3H system at different pH values.

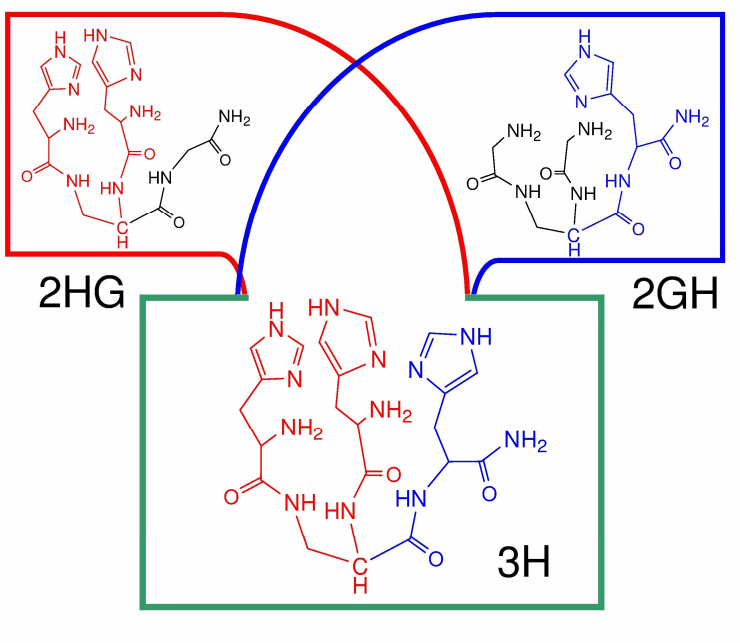

Figure 1. Graphical presentation of combining two 2,3-diaminopropionic branched peptides in one that contains both metal binding histidine domains. The two N-terminals peptide arms are marked with red and the C-terminal arm is marked with blue. 2HG = H-His-Dap(H-His)-Gly-NH_2, 2GH = H-Gly-Dap(H-Gly)-His-NH_2 and 3H = H-His-Dap(H-His)-His-NH_2 peptides.

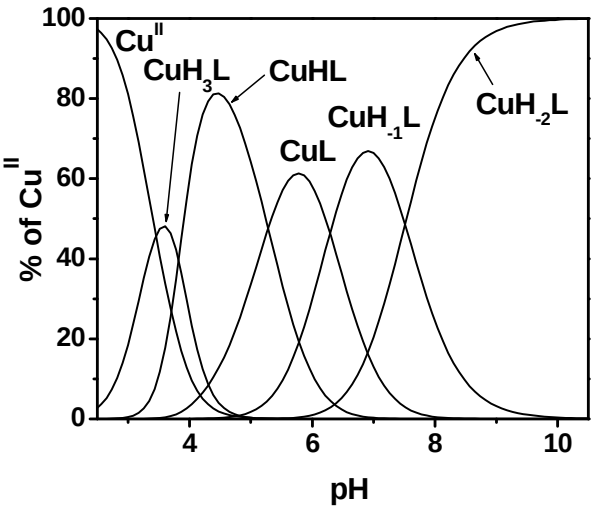

Figure 2. Speciation diagram for the system containing Cu^{II} and 3H, $[Cu^{II}] = 1 \times 10^{-3}$ M, $1Cu^{II}$: 1L (where L = 3H).

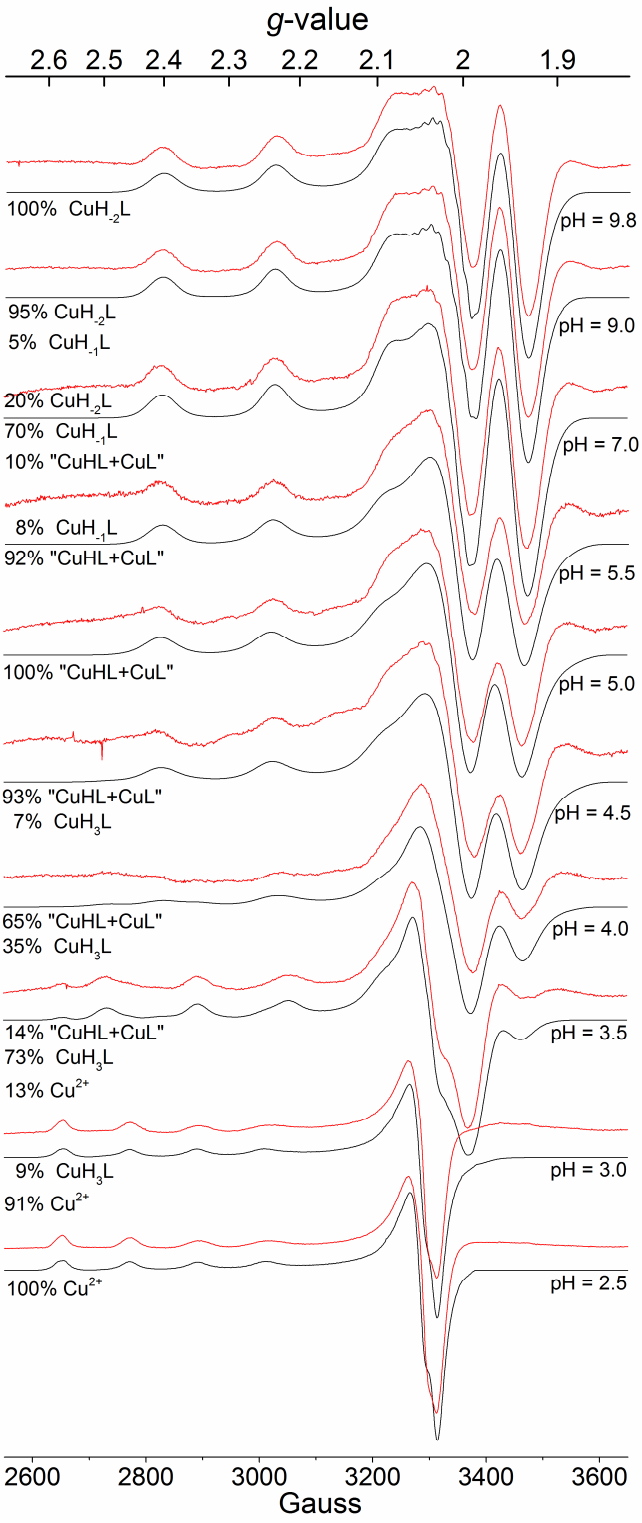

Figure 3. Experimental (red) and simulated (black) EPR spectra at different pH for the Cu^{II} : 3H system.

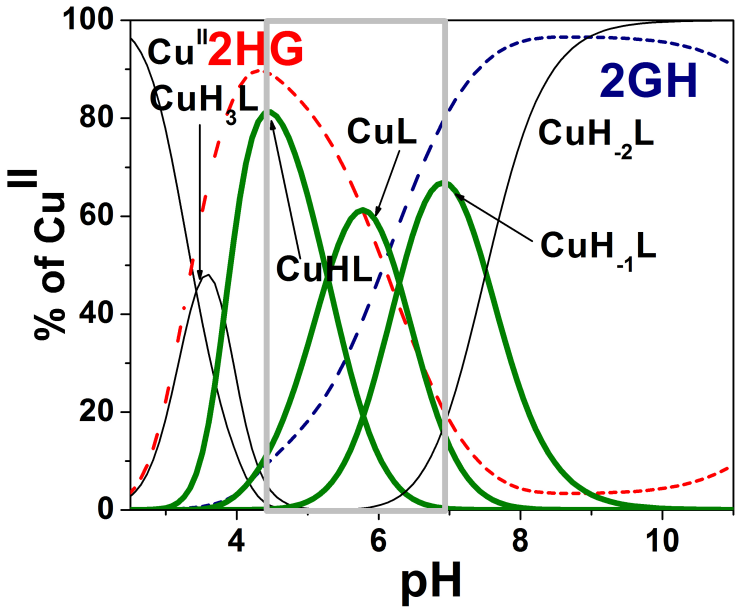

Figure 4. Speciation diagram for Cu^{II} and 3H, dashed lines show curves of competition for Cu^{II} between the ligands 2HG (red), 2GH (blue). The gray rectangle illustrates the region where the switching between branches that participate in Cu^{II} binding takes place as the respective complex species marked with green (CuHL, CuL and $CuH_{-1}L$) occur (the conditions of speciation and competition diagram: $[Cu^{II}]$ = [3H] = 1×10^{-3} M, $[Cu^{II}]$ = [2GH] = [2HG] = 1×10^{-3} M respectively).

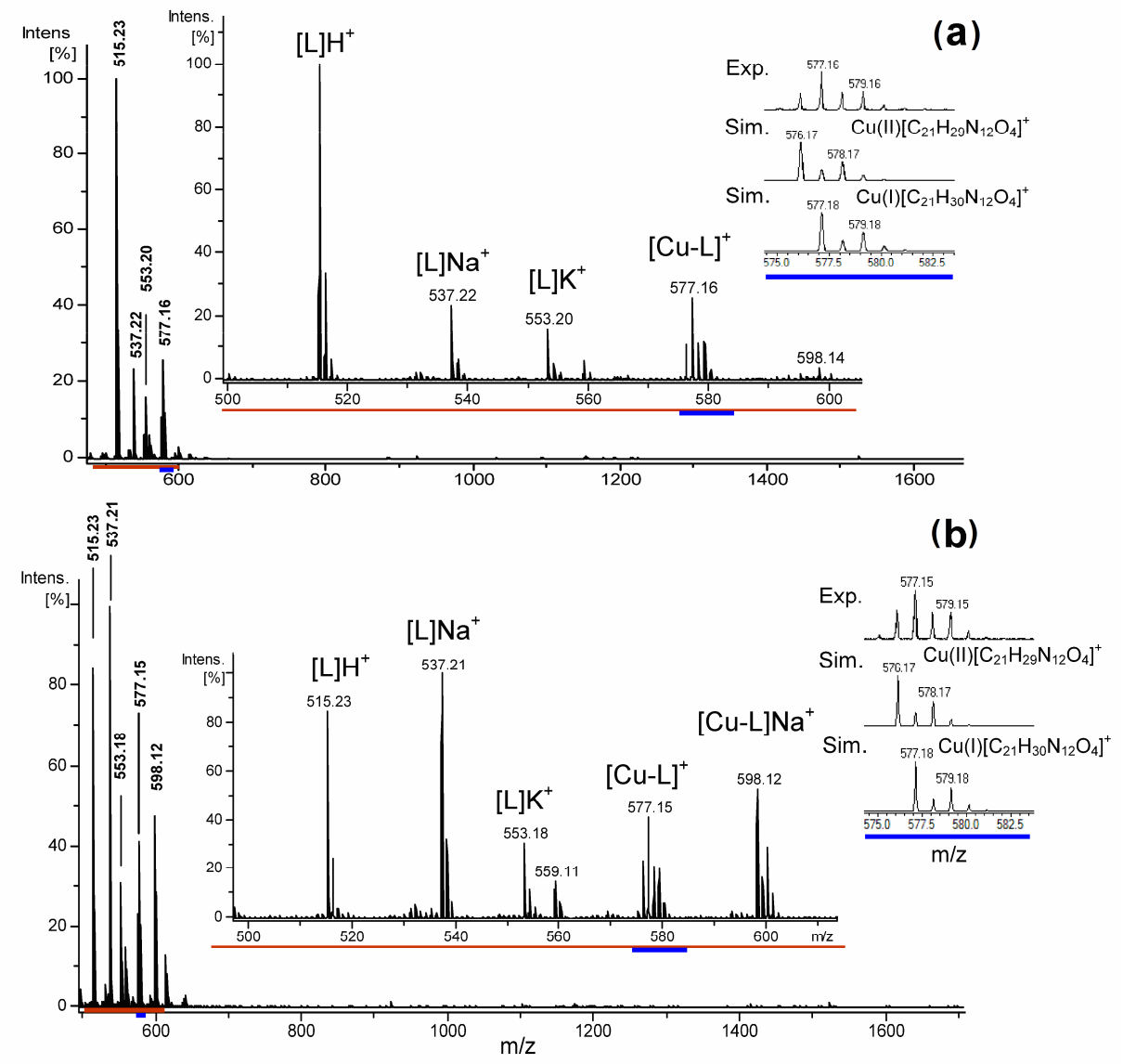

Figure 5. The (+)ESI-MS spectrum of the Cu^{II} – L mixture at pH 6.8: (a) the Cu^{II} : L ratio was 0.4 : 1.0 and (b) the Cu^{II}: L ratio was 0.7 : 1.0 ($C_L = 0.8 \times 10^{-4}$ M, where L = 3H). Respective, blown up regions of spectra are marked with red and blue.

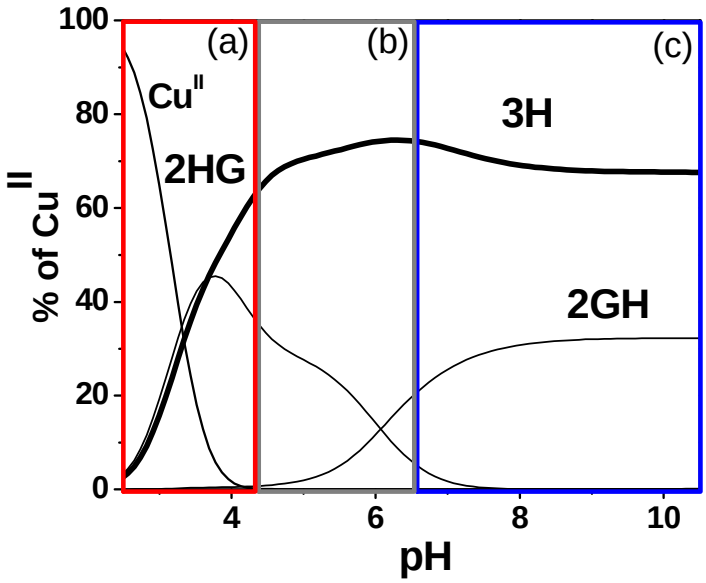

Figure 6. Competition plot showing the distribution of Cu^{II} between 2GH, 2HG and 3H as a function of pH, $[Cu^{II}]$ = [2GH] = [2HG] = [3H] = 1×10^{-3} M. Partitions denote those pH regions where spectroscopic parameters of 3H could be recognized as: a) similar to 2HG (red), b) 3H specific (2HG and 2GH competitive region), c) similar to 2HG (blue).

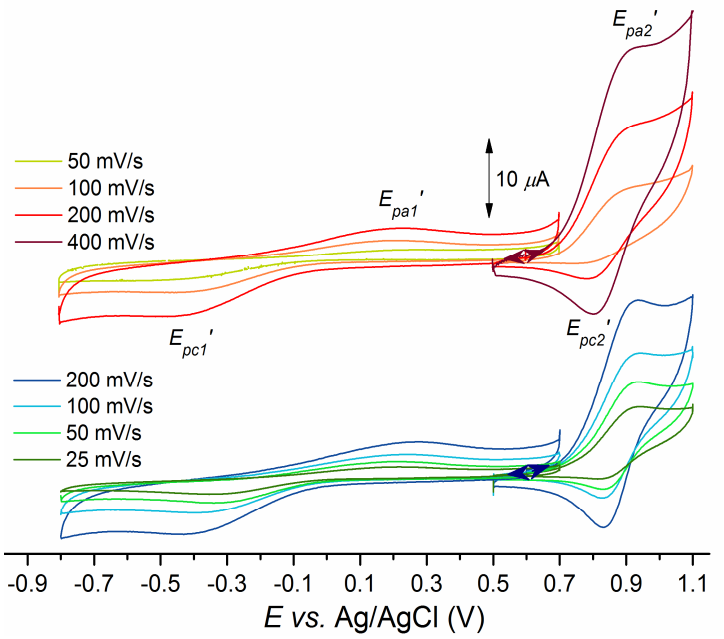

Figure 7. Cyclic voltammograms of the Cu-3H system (2 mM in water, 0.1 M $NaClO_4$, under argon at 25°C) at pH 7.0 (bottom) and at pH 8.0 (top) plotted on the same scale. The initial potential is 0.6 V for scans to both the anodic and cathodic directions (see blue and brown arrowheads).

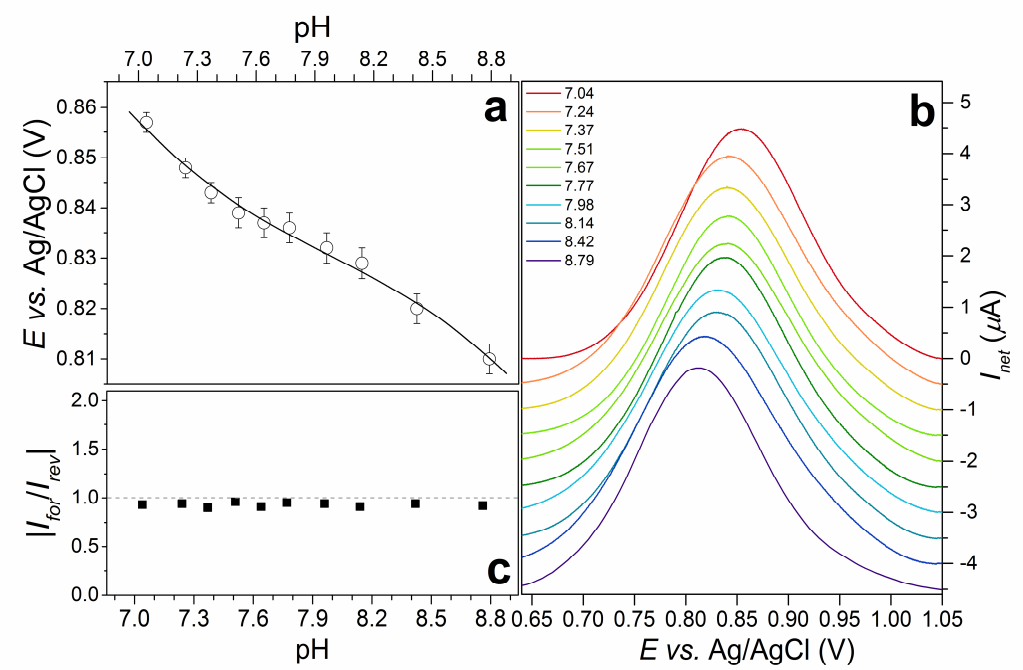

Figure 8. (a) $Cu^{III/II}$ net formal potentials (E_{net}) determined by square-wave voltammetry (SWV) and plotted as a function of pH. The solid line represents a nonlinear regression curve fit to eq. (2) (R^2 = 0.9857, for parameters see Table 3). (b) Baseline corrected net current SW voltammograms of the Cu-3H system between pH 7.04 and 8.79. The potentials in Fig. 7a correspond to E_{net} of the baseline corrected net current traces, $I_{net} = I_{for} - I_{rev}$, where forward means the current response to the oxidation pulse while reverse to the reduction pulse. (c) Plot of the ratio of I_{for} and I_{rev} components as a function of pH. SWV conditions: 0.7 mM Cu-3H, 100 mM $NaClO_4$, temperature 25.0±0.1 °C, tp = 10 ms (f = 50 Hz), step potential 0.2 mV, SW pulse amplitude 25 mV, 0.072 cm^2 GC working electrode, ~2 cm^2 Pt auxiliary electrode and Ag/AgCl (3 M KCl) reference electrode. All experiments were conducted under an Ar blanketing atmosphere, where O_2 concentration was < 2 μM